

Laser-cooling ^{88}Sr to microkelvin temperature with an integrated-photonics system

Andrew R. Ferdinand,^{1,2} Zheng Luo^{1,2}, Sindhu Jammi,^{1,2} Zachary Newman,³ Grisha Spektor,^{1,2,3} Okan Koksal^{1,4}, Parth B. Patel,⁵ Daniel Sheredy,⁵ William Lunden,⁵ Akash Rakholia,⁵ Travis C. Briles^{1,2}, Wenqi Zhu^{1,4}, Martin M. Boyd,⁵ Amit Agrawal^{1,4}, and Scott B. Papp^{1,2,*}

¹Time and Frequency Division, National Institute of Standards and Technology (NIST), Boulder, Colorado 80305, USA

²Department of Physics, University of Colorado, Boulder, Colorado 80309, USA

³Octave Photonics, Louisville, Colorado 80027, USA

⁴Microsystems and Nanotechnology Division, NIST, Gaithersburg, Maryland 20899, USA

⁵Vector Atomic, Inc., Pleasanton, California 94588, USA



(Received 8 May 2024; revised 27 December 2024; accepted 17 January 2025; published 21 March 2025)

We report on generating a magneto-optical trap (MOT) of ^{88}Sr atoms at microkelvin temperature, using integrated-photonics devices. With metasurface optics integrated on a fused-silica substrate, we generate six-beam circularly polarized counterpropagating MOTs on the blue broad-line (461-nm) and red narrow-line (689-nm) Sr cooling transitions without bulk optics. By use of a diverging beam configuration, we create up to 10-mm-diameter MOT beams at the trapping location. To frequency stabilize and linewidth narrow the cooling lasers, we use fiber-packaged integrated nonlinear waveguides to spectrally broaden a frequency comb. The ultracoherent supercontinuum of the waveguides covers 650–2500 nm, enabling phase locks of the cooling lasers to hertz-level linewidth. Our work highlights the possibility of simplifying the preparation of an ultracold ^{88}Sr gas for an optical-lattice clock with photonic devices. By implementing a timing sequence for control of the MOT lasers and the quadrupole magnetic field gradient, we collect atoms directly from a thermal beam into the blue MOT and continuously cool into a red MOT with dynamic detuning and intensity control. There, the red-MOT temperature is as low as 2 μK and the overall transfer efficiency is up to 16%. We characterize this sequence, including an intermediate red MOT with modulated detuning.

DOI: 10.1103/PhysRevApplied.23.L031002

Access to ultracold samples of alkaline-earth atomic species promotes development in optical-lattice clocks [1], searches for fundamental physics [2], exploration of quantum matter [3], and quantum simulation and computation [4]. Species such as Sr offer a variety and richness of atomic transitions that facilitate numerous physical interactions and controls with optical fields. A broad-linewidth transition at 461 nm enables robust laser cooling from a vapor or atomic beam source, referred to as a blue magneto-optical trap (MOT). The spectrally narrow intercombination transitions allow for further cooling to microkelvin temperature at 689 nm, referred to as a red MOT, and provide high-precision high-stability frequency reference at 698 nm for optical clocks [5].

Various directions in integrated photonics have been explored for laser cooling and trapping of alkali atoms [6–14]. The complexity of controlling and manipulating Sr gases leads to challenges in the development of systems

suitable for applications beyond laboratory experiments. Employing Sr MOTs requires addressing the atoms with a complex three-dimensional beam geometry with both 461-nm and 689-nm laser wavelengths in a dynamic experimental sequence. Moreover, experiments require a source of Sr vapor and an ultrahigh-vacuum environment. Laboratory-type strontium systems generally implement an MOT-beam geometry with manually aligned tabletop bulk optic systems. Cooling on the narrow-line transition requires precise frequency stabilization, which is complicated by low vapor pressure in room-temperature cells. Furthermore, the light must be of narrow enough linewidth to address the atomic transitions. Laboratory systems typically consist of high-finesse bulk optical-reference cavities and complex arrangements of highly nonlinear fiber and nonlinear crystals. The incompatibility of specialized and bulky laboratory solutions for transportable cold-atom systems points to the development of alternative technologies [15]. Since generating large-diameter laser beams is already bulky, there is motivation to develop integrated photonics technologies [10,16–18]. Also, simplifying atomic physics systems motivates the

*Contact author: scott.papp@nist.gov

development of laser sources with integrated photonics [19–23]

Here, we report on a system to create a sample of ^{88}Sr atoms laser cooled to microkelvin temperature with integrated-photonics devices. Our system uses metasurface (MS) optics integrated on a common substrate to generate a complete multiwavelength three-dimensional set of MOT beams without the use of bulk optics. The metasurface-optics system implements beam routing, polarization, pointing, and divergence control for both sets of MOT beams. We frequency stabilize the cooling lasers to a frequency-comb supercontinuum generated with fiber-packaged integrated nonlinear waveguides. The supercontinuum provides high-power modes at 689 nm, 698 nm, 813 nm, and 922 nm to reference all the lasers needed in an Sr optical clock. The reduced complexity of our integrated-photonics approach eliminates barriers to production of robust ultracold atom samples for applications outside of specialized laboratories. Our experiments demonstrate an integrated photonics system capable of cooling alkaline-earth gases to microkelvin temperature with sufficient transfer efficiency for adoption in scalable optical clocks and quantum sensors.

The apparatus we use, including MS optics, magnetic field coils, the waveguide supercontinuum, the vacuum chamber, and the timing sequence to laser cool ^{88}Sr , is introduced in Fig. 1. We create the 12-beam, free-space configuration of 461-nm and 689-nm MOT beams with metasurface optics, which are integrated on two fused-silica substrates [16]. By illuminating each MS optic with light directly expanding from a polarization-maintaining fiber, we simultaneously engineer the optical phase profile for a near-arbitrary pointing angle, beam divergence, and polarization [see Fig. 1(a)]. This integrated approach simplifies the formation of MOT beams because each metasurface optic performs the function of mirrors, lenses, beam splitters, and wave plates. To implement the MS system with Sr atoms, we have developed a flattened titanium ultrahigh-vacuum chamber with large view ports to accept the beams from the MS substrates. Moreover, we load Sr atoms into the MOT from a collimated thermal-atom beam, Doppler slowed on the $^1\text{S}_0 \rightarrow ^1\text{P}_1$ transition.

Our propagation phase MSs [24] are arrays of subwavelength TiO_2 nanopillars that impart a phase shift on the optical beam. The phase shift varies, depending on the dimensions of the intercepted nanopillar. We numerically simulate these phase shifts for various pillar geometries and collect them into a library. Then, we position pillars at locations at which the imparted phase shift matches that required by the desired phase profile. The 12 metasurfaces are partitioned onto two 3-in. fused-silica wafers that are placed symmetrically about our compact vacuum chamber, using mechanical fixtures. The MS optics deflect each beam at 45° toward the trap center. We adjust the sizes of the 461-nm and 689-nm trapping beams at the trap center

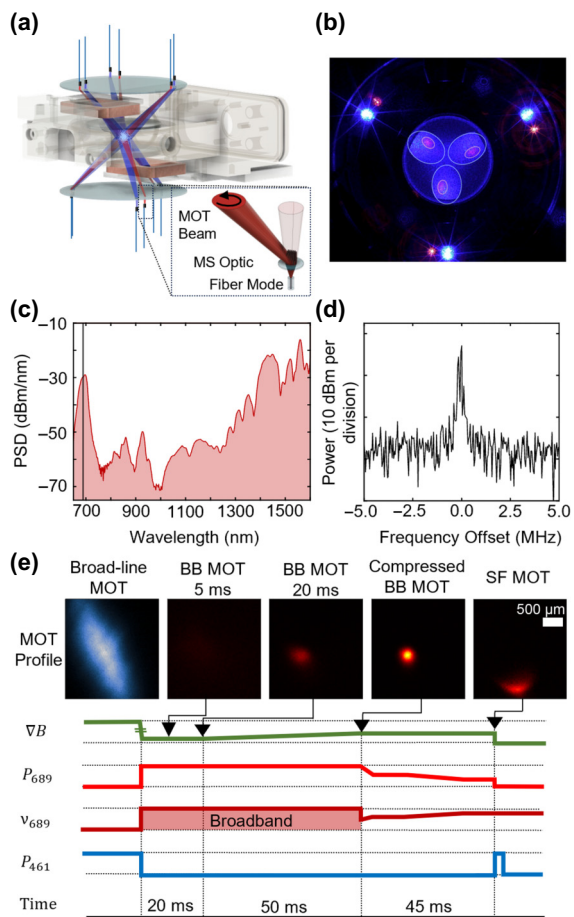


FIG. 1. The Sr system with integrated photonics. (a) The metasurface-based system. The inset depicts the generation of an MOT beam with a multifunctional MS optic. (b) A multiwavelength MOT-beam cross section 7.5 mm from the trap center. (c) The supercontinuum power spectral density (PSD) with a dispersive wave at the target 689-nm wavelength. (d) The heterodyne beat of the 689-nm cooling laser and the supercontinuum. (e) The experimental sequence, with selected false-color MOT images, including broadband (BB) and single-frequency (SF) narrow-line MOTs.

by varying the effective focal length through the quadratic term in the phase profile or by changing the mode diameter at the input to the MS. For the first stage of laser cooling, we choose a relatively large beam diameter at the atoms ($d = 1 \text{ cm}$) to create a large trap volume and maximize the total trapped-atom number [25,26]. For the second stage of laser cooling, we choose a smaller beam diameter of $d = 3 \text{ mm}$, which is dictated largely by our available laser power and the laser intensity required to effectively cool from our millikelvin blue-MOT temperature in the red MOT.

An essential feature of our system is the integration of MSs for multiwavelength laser cooling on a single substrate. In Fig. 1(b), we present a horizontal cross section of the 461-nm and 689-nm beams generated by a single substrate at a distance 7.5 mm below the trap center. The

outlines of the beams are digitally emphasized for clarity. The MSs are arranged with a minimal azimuthal offset of 10° , which is crucial for maintaining alignment with the magnetic field for proper operation of our MOT at both wavelengths. This clocking angle can be seen in the residual light from the fibers that is transmitted through the wafer but undeflected by the MSs [see the outer perimeter of Fig. 1(b)].

We frequency stabilize the red- and blue-MOT lasers to a frequency-comb supercontinuum, generated with fiber-coupled integrated nonlinear waveguide modules. Dispersion engineering via the waveguide geometry allows us to tailor the generated supercontinuum spectra for a high power spectral density (PSD) in target spectral bands, i.e., 700 nm and 922 nm. The modules are composed of a 12-mm-long tantalum waveguide on a silicon chip [27] with 800-nm thickness, 1800-nm waveguide width, and silicon oxide top cladding that can be selectively removed from a portion of the waveguide to facilitate group-velocity dispersion engineering. We create inverse tapers at the chip edge with a 180-nm critical dimension to enable low-insertion-loss packaging to polarization-maintaining optical fiber. An amplified 1550-nm mode-locked fiber laser seeds the supercontinuum generation process. This mode-locked laser is carrier-envelope offset locked with a separate tantalum waveguide and periodically poled lithium niobate (PPLN) integrated module. We phase lock the mode-locked laser offset and repetition frequencies with respect to a hydrogen-maser reference and an ultrastable 1550-nm optical reference cavity, respectively. The selection of the optical-frequency reference represents a compromise between the size of the cavity, which dictates thermal-noise contributions and hence the frequency noise of the reference, and the overall size and complexity of the cavity system, potentially including cryogenic cooling, vibration mitigation, temperature stabilization. Our module to generate supercontinuum for locking the narrow-line cooling laser creates a dispersive wave with -30 dBm/nm PSD at the target 689-nm wavelength, as seen in Fig. 1(c) [27–29]. To phase lock the red- and blue-MOT lasers, we obtain heterodyne beats with the supercontinuum and implement standard electronic phase-locked loops. An example unlocked heterodyne beat of the supercontinuum and our 689-nm laser is given in Fig. 1(d). The signal-to-noise ratio of the heterodyne beat-note signal in the gigahertz frequency range is sufficient for coherent digital frequency division as part of our electronic phase-locking system [28,30]. Hence, our optical phase-locked loop stabilizes the 689-nm laser frequency with a negligible excess-noise contribution compared to the frequency-comb supercontinuum. The MOGLabs 689-nm laser system that we use provides low intrinsic frequency fluctuations consistent with an external-cavity diode laser. Out-of-loop measurements with an independent frequency comb indicate a hertz-level linewidth of the locked laser, sufficient

for cooling on the 7.5-kHz-linewidth atomic intercombination transition of Sr. This additionally indicates that the coherence of our supercontinuum is maintained spanning over a octave and into the visible wavelength range, motivating its use for laser stabilization in applications beyond specialized laboratory settings.

Achieving microkelvin temperature with Sr requires addressing both cooling transitions in a dynamic experimental sequence [see Fig. 1(e)]. In the first phase of the sequence, we load and cool atoms in the blue MOT from a thermal-atom beam from a conventional oven, assisted by our Doppler slowing. The magnetic field gradient along the axis between the coils ∇B is 50 G/cm. We repump atoms that decay from the excited state into the 3P_J manifold with 707-nm and 679-nm lasers. The blue MOT cools atoms to millikelvin temperature, fundamentally limited by the Doppler limit $T_D = \hbar\Gamma/2k_B = 0.7$ mK [31], where \hbar is the reduced Planck's constant, k_B is Boltzmann's constant, and Γ is the natural linewidth of the transition. We transfer the atoms to the red MOT for further cooling on the 7.5-kHz intercombination transition. The much lower Doppler limit of $T_D = 0.2$ μK is important for lattice loading and precision spectroscopy. However, the smaller linewidth and larger g factor necessitate dynamic control of the magnetic field gradient, laser power, and laser frequency. During the first period of cooling on the narrow-line transition, frequency modulation of the 689-nm cooling light allows the laser to address all of the atomic velocities comprising the millikelvin-temperature blue MOT, and we refer to this as the broadband (BB) MOT. Reducing the magnetic field gradient to $\nabla B = 5$ G/cm optimizes scattering and improves the transfer efficiency into the BB MOT. After 20 ms of BB cooling in the lower magnetic field gradient, we ramp the gradient to 10 G/cm over 50 ms, spatially compressing the atom cloud to the final BB MOT. After the BB MOT, we extinguish the frequency modulation to implement a single-frequency (SF) final cooling stage. During this cooling stage, we ramp down the cooling laser intensity and detuning over 45 ms to reduce the scattering rate and further compress the atom cloud. This step reduces the temperature and increases the phase-space density [32]. At a sufficiently low temperature, laser intensity, and spatial confinement, the gravitational force on the atoms becomes a non-negligible contributor to the cooling potential. Therefore, the MOT shape evolves to an apparent crescent as the atoms settle near the bottom of the ellipsoidal potential [31] [see the MOT profile panel in Fig. 1(e)]. We note that there have been no device failures in operation of the integrated-photonics systems for laser stabilization and MOT-beam formation over approximately 2 years. In the remainder of the letter, we present characterizations of our BB MOT and SF MOTs.

In Fig. 2, we present the characterization of our BB MOT. The transfer efficiency from the blue MOT to the BB MOT depends on the spectral parameters of the 689-nm

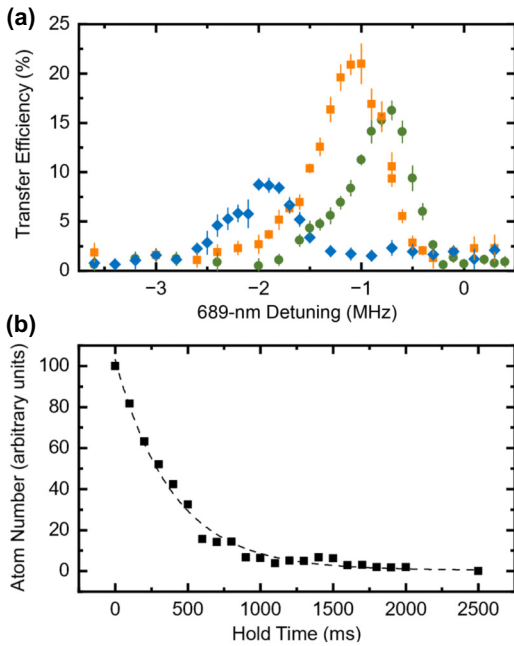


FIG. 2. BB MOT characterization. (a) The transfer efficiency with $1-\sigma$ error bars versus detuning for three values of the modulation frequency range δ_{FM} : 880 kHz (green circles), 1760 kHz (orange squares), and 3520 kHz (blue diamonds). The bars indicate the standard deviation. (b) The atom number versus time at the end of the BB-MOT sequence.

laser, including the detuning from the atomic transition and the laser linewidth broadening from frequency modulation. Effectively configured spectral parameters allow the cooling light to address the full velocity distribution of atoms in the blue MOT while maintaining a sufficient PSD to trap the atoms. In our experiments, we modulate the laser at $f_{\text{mod}} = 50$ kHz, creating sidebands across a controllable frequency range, δ_{FM} , such that the laser addresses each accessible atomic velocity class once within an atomic lifetime $\tau = \Gamma^{-1}$. In Fig. 2(a), we present the BB-MOT transfer efficiency as a function of the detuning for three values of δ_{FM} : 880 kHz (green), 1760 kHz (orange), and 3520 kHz (blue). The data exhibit similar relationships between transfer efficiency, detuning, and δ_{FM} . The maximum transfer efficiency occurs when the detuning and δ_{FM} are set such that the maximum frequency sampled by the laser is a slightly lower frequency than the atomic resonance. We achieve a maximum transfer efficiency of 21% with 1-MHz detuning and $\delta_{\text{FM}} = 1760$ kHz, which is consistent with previous measurements on free-space red MOTs [33]. We characterize the BB-MOT lifetime by observing the decay in the atom number over time [see Fig. 2(b)]. An exponential fit (dashed) indicates a lifetime of (400 ± 20) ms, where the uncertainty is the standard error of the fit.

In Fig. 3, we present a characterization of the SF MOT at the conclusion of our experimental sequence. Here, we fix the red-MOT parameters except for the intensity,

which we vary to explore the low-photon-scattering regime that coincides with lowest temperature. We measure the temperature of the MOT with a time-of-flight technique, stroboscopically recording the atom-cloud size expansion after turning off the trap. At the end of the expansion time, a CMOS camera images the atom-cloud fluorescence from a 125- μ s pulse of 461-nm MOT light, collecting a column-integrated signal from the cloud. In Fig. 3(a), we present such a measurement, in which each data point corresponds to a variation in the free-expansion time and free fall under gravity. Fitting the cloud radius σ as a function of the expansion time gives the MOT temperature through the relationship $\sigma(t) = \sqrt{\sigma(t=0)^2 + k_B T/m \times t^2}$, where T is the temperature and m is the atomic mass. We characterize the temperature in the two observed directions, horizontal (light red triangle) and vertical (dark red square), since the nonconservative forces of an MOT do not completely thermalize the energy distribution of the trapped gas. Our system achieves an average MOT temperature as low as 2 μ K, which is most likely cold enough to permit future experiments that load a magic wavelength optical lattice with high efficiency. The insets show MOT images at the minimum and maximum expansion times of the data set. Critically, our system produces atoms with microkelvin temperature, reasonable transfer efficiencies,

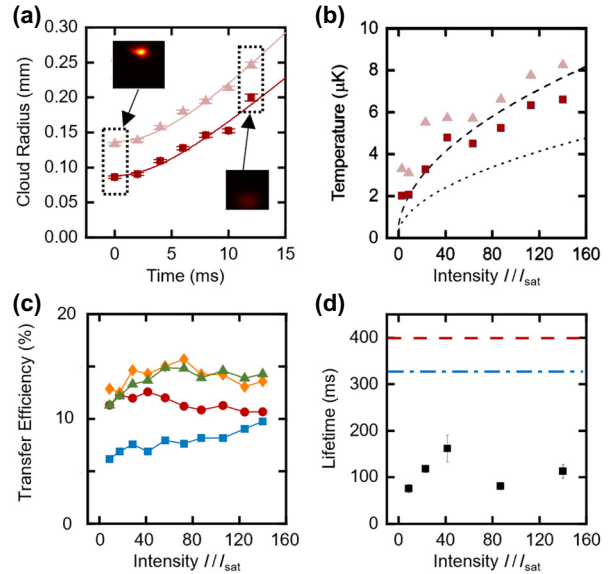


FIG. 3. SF-MOT characterization. (a) The time-of-flight expansion of the horizontal (light red triangle) and vertical (dark red square) cloud radius; the bars represent $1-\sigma$ variations in repeated measurements. (b) The SF-MOT temperature with I/I_{sat} ; the dashed lines indicate the theoretical temperature $T = N_r \times \hbar \Gamma(I)/2k_B$ with $N_r = 2.1$ (dotted) and $N_r = 2.1\sqrt{3}$ (dashed). (c) The transfer Efficiency with I/I_{sat} for $\Delta_{\text{final}} = -333$ kHz (blue square), $\Delta_{\text{final}} = -500$ kHz (red circle), $\Delta_{\text{final}} = -667$ kHz (orange), and $\Delta_{\text{final}} = -750$ kHz (green). (d) The SF-MOT lifetime versus the intensity (black square); the blue-MOT and BB-MOT lifetimes are shown as a dash-dotted blue line and a dashed red line, respectively.

and a trapping lifetime that in principle enables loading into a magic wavelength optical lattice for clock spectroscopy of the $^1\text{S}_0 \rightarrow ^3\text{P}_0$ transition.

In the regime of large detuning relative to the power-broadened transition linewidth, the equilibrium of the trapping forces of the MOT and the Zeeman-induced detuning variation balance against gravity. Thermodynamic modeling of narrow-line cooling predicts an SF-MOT temperature $T = N_r \times \hbar\Gamma(I)/2k_B$, analogous to the Doppler limit, where \hbar is Planck's constant, $\Gamma(I) = \Gamma \sqrt{1 + I/I_{\text{sat}}}$ is the power-broadened transition linewidth, I is the single-beam peak intensity, $I_{\text{sat}} = 3 \mu\text{W}/\text{cm}^2$ is the saturation intensity of the transition, and N_r is an overall scaling factor [31]. In this regime of laser cooling, the final temperature of the MOT is primarily dependent on the laser intensity. Modeling of a traditional cubic MOT geometry, in which a single beam provides the force counteracting gravity, predicts a weakly intensity-dependent $N_r \approx 2.1$ [31].

We systematically vary the SF-MOT intensity to search for the lowest temperature [see Fig. 3(b)], with the dotted black line indicating the temperature predicted with $N_r = 2.1$. The overall trend of the data indicates that the intensity-dependent temperature of the SF MOT reaches approximately $2 \mu\text{K}$ at $I/I_{\text{sat}} = 5$. However, in our system with three MOT beams oriented with vertical components, the temperature dependence with $\Gamma(I)$ is consistent with $\sqrt{3}$ larger laser power. Indeed, scaling the temperature theory according to $N_r = 2.1\sqrt{3}$ is consistent with our observations [see the dashed line in Fig. 3(b)]. These data highlight a trade space of system design with integrated photonics, which largely constrains beam emission to a planar geometry, opening light-atom interactions to complexity from imperfect matching of polarization, magnetic fields [15], the gravitational field, and geometrical imperfections that cause atoms to scatter light from additional MOT beams in the equilibrium position of an SF red MOT. Indeed, our entire MS beam-delivery system is assembled with no free-space optics and no adjustments. While we do not saturate the theoretical limit of achievable SF-MOT temperature, our results are sufficient to load atoms into an optical lattice, which we will characterize in a future report.

In Fig. 3(c), we explore the transfer efficiency from the blue MOT to the SF MOT as a function of the laser intensity and detuning at the conclusion of the experimental sequence. We measure the transfer efficiency for four final detunings Δ_{final} : -333 kHz (blue), -500 kHz (red), -667 kHz (orange), and -750 kHz (green). We observe a transfer efficiency between 11% and 16% without a significant intensity dependence, except for the $\Delta_{\text{final}} = -333 \text{ kHz}$ detuning. At this value of Δ_{final} , we see an approximately linear increase in transfer efficiency with intensity, peaking at 10% at $I = 140 I_{\text{sat}}$. We measure the lifetime of the SF MOT to be between 80 ms and 160 ms [Fig. 3(d)]. Our blue MOT holds several million ^{88}Sr atoms, which we estimate based on scattering from all of the blue-MOT

laser beams and collection onto a calibrated avalanche photodiode. Operationally, the atom-number calibration is influenced by the small collection solid angle and the confined access to measure the MOT-beam power *in situ* with our compact alignment-free prototype system. Moreover, the Sr beam source without a Zeeman slower used in our experiments limits the available number of atoms that can be addressed by the slowing and MOT beams. Taking these factors into account, the overall atom number of approximately 3×10^5 and the temperature that we transfer to the SF MOT are promising for implementation of optical-lattice loading and clock-transition spectroscopy, particularly in comparison to recent portable clock systems that operate with similar parameters. Demonstrations of transportable optical-lattice clocks without integrated photonics provide a benchmark for the required atom number and temperature [34].

In conclusion, our work demonstrates laser cooling of ^{88}Sr atoms to microkelvin temperature, using an integrated-photonics system. Through the integration of metasurface optics on a fused-silica substrate, we demonstrate both broad- and narrow-line cooling free from bulk optics or alignment of individual MOT beams. Our system employs fiber-packaged integrated nonlinear waveguides to spectrally broaden a frequency comb, enabling frequency stabilization and linewidth narrowing of the cooling lasers. Our findings eliminate barriers to employing ultracold atomic physics systems.

Acknowledgments. This work was supported by Defense Advanced Research Projects Agency (DARPA) A-Phi FA9453-19-C-0029, Air Force Office of Scientific Research (AFOSR) FA9550-20-1-0004 Project No. 19RT1019, National Science Foundation (NSF) Quantum Leap Challenge Institute (QLCI) Award No. OMA—2016244, and NIST. This work is a contribution of the U.S. government and is not subject to copyright. Trade names provide information only and not an endorsement.

Data Availability. The data from this paper, which are all shown in the figures, are available upon reasonable request from the authors. The data are not publicly available because a suitable repository does not exist.

-
- [1] A. D. Ludlow, M. M. Boyd, J. Ye, E. Peik, and P. O. Schmidt, Optical atomic clocks, *Rev. Mod. Phys.* **87**, 637 (2015).
 - [2] M. Safronova, D. Budker, D. DeMille, D. F. J. Kimball, A. Derevianko, and C. W. Clark, Search for new physics with atoms and molecules, *Rev. Mod. Phys.* **90**, 025008 (2018).
 - [3] M. J. Martin, M. Bishop, M. D. Swallows, X. Zhang, C. Benko, J. von Stecher, A. V. Gorshkov, A. M. Rey, and J. Ye, A quantum many-body spin system in an optical lattice clock, *Science* **341**, 632 (2013).
 - [4] A. M. Kaufman and K.-K. Ni, Quantum science with optical tweezer arrays of ultracold atoms and molecules, *Nat. Phys.* **17**, 1324 (2021).

- [5] T. L. Nicholson, S. L. Campbell, R. B. Hutson, G. E. Marti, B. J. Bloom, R. L. McNally, W. Zhang, M. D. Barrett, M. S. Safronova, G. F. Strouse, W. L. Tew, and J. Ye, Systematic evaluation of an atomic clock at 2×10^{-18} total uncertainty, *Nat. Commun.* **6**, 6896 (2015).
- [6] E. Imhof, B. K. Stuhl, B. Kasch, B. Kroese, S. E. Olson, and M. B. Squires, Two-dimensional grating magneto-optical trap, *Phys. Rev. A* **96**, 033636 (2017).
- [7] L. Zhu, X. Liu, B. Sain, M. Wang, C. Schlickriede, Y. Tang, J. Deng, K. Li, J. Yang, M. Holynski, S. Zhang, T. Zentgraf, K. Bongs, Y.-H. Lien, and G. Li, A dielectric metasurface optical chip for the generation of cold atoms, *Sci. Adv.* **6**, eabb6667 (2020).
- [8] W. R. McGehee, W. Zhu, D. S. Barker, D. Westly, A. Yulaev, N. Klimov, A. Agrawal, S. Eckel, V. Aksyuk, and J. J. McClelland, Magneto-optical trapping using planar optics, *New J. Phys.* **23**, 013021 (2021).
- [9] T.-W. Hsu, W. Zhu, T. Thiele, M. O. Brown, S. B. Papp, A. Agrawal, and C. A. Regal, Single-atom trapping in a metasurface-lens optical tweezer, *PRX Quantum* **3**, 030316 (2022).
- [10] A. Isichenko, N. Chauhan, D. Bose, J. Wang, P. D. Kunz, and D. J. Blumenthal, Photonic integrated beam delivery for a rubidium 3D magneto-optical trap, *Nat. Commun.* **14**, 3080 (2023).
- [11] D. S. Barker, P. K. Elgee, A. Sitaram, E. B. Norrgard, N. N. Klimov, G. K. Campbell, and S. Eckel, Grating magneto-optical traps with complicated level structures, *New J. Phys.* **25**, 103046 (2023).
- [12] M. Jin, X. Zhang, X. Liu, C. Liang, J. Liu, Z. Hu, K. Li, G. Wang, J. Yang, L. Zhu, and G. Li, A centimeter-scale dielectric metasurface for the generation of cold atoms, *Nano Lett.* **23**, 4008 (2023).
- [13] J. Pick, R. Schwarz, J. Kruse, C. Lisdat, and C. Klempert, Compact structures for single-beam magneto-optical trapping of ytterbium, *Rev. Sci. Instrum.* **95**, 073201 (2024).
- [14] J. Pick, J. Voß, S. Hirt, J. Kruse, T. Leopold, R. Schwarz, and C. Klempert, Low-power microstructured atomic oven for alkaline-earth-like elements, *Phys. Rev. Appl.* **23**, 014020 (2025).
- [15] S. Bondza, C. Lisdat, S. Kroker, and T. Leopold, Two-color grating magneto-optical trap for narrow-line laser cooling, *Phys. Rev. Appl.* **17**, 044002 (2022).
- [16] S. Jammi, A. R. Ferdinand, Z. Luo, Z. L. Newman, G. Spektor, J. Song, O. Koksal, A. V. Rakholia, W. Lunden, D. Sheredy, P. B. Patel, M. M. Boyd, W. Zhu, A. Agrawal, T. C. Briles, and S. B. Papp, Three-dimensional, multi-wavelength beam formation with integrated metasurface optics for Sr laser cooling, *Opt. Lett.* **49**, 6013 (2024).
- [17] C. Ropp, W. Zhu, A. Yulaev, D. Westly, G. Simelgor, A. Rakholia, W. Lunden, D. Sheredy, M. M. Boyd, S. Papp, A. Agrawal, and V. Aksyuk, Integrating planar photonics for multi-beam generation and atomic clock packaging on chip, *Light Sci. Appl.* **12**, 83 (2023).
- [18] D. J. Blumenthal, A. Isichenko, and N. Chauhan, Enabling photonic integrated 3D magneto-optical traps for quantum sciences and applications, *Opt. Quantum* **2**, 444 (2024).
- [19] L. Stern, W. Zhang, L. Chang, J. Guo, C. Xiang, M. A. Tran, D. Huang, J. D. Peters, D. Kinghorn, J. E. Bowers, and S. B. Papp, Ultra-precise optical-frequency stabilization with heterogeneous III-V/Si lasers, *Opt. Lett.* **45**, 5275 (2020).
- [20] K. Liu, N. Chauhan, J. Wang, A. Isichenko, G. M. Brodnik, P. A. Morton, R. O. Behunin, S. B. Papp, and D. J. Blumenthal, 36 Hz integral linewidth laser based on a photonic integrated 4.0 m coil resonator, *Optica* **9**, 770 (2022).
- [21] W. Zhang, L. Stern, D. Carlson, D. Bopp, Z. Newman, S. Kang, J. Kitching, and S. B. Papp, Ultranarrow linewidth photonic-atomic laser, *Laser Photon. Rev.* **14**, 1900293 (2020).
- [22] W. Zhang, E. Kittlaus, A. Savchenkov, V. Iltchenko, L. Yi, S. B. Papp, and A. Matsko, Monolithic optical resonator for ultrastable laser and photonic millimeter-wave synthesis, *Commun. Phys.* **7**, 1 (2024).
- [23] C. A. McLemore, N. Jin, M. L. Kelleher, Y. Luo, D. Lee, Y. Liu, T. Nakamura, D. Mason, P. Rakich, S. A. Diddams, and F. Quinlan, Fiber-coupled 2 mL vacuum-gap Fabry-Perot reference cavity for portable laser stabilization, *Opt. Lett.* **49**, 4737 (2024).
- [24] Q. Fan, M. Liu, C. Zhang, W. Zhu, Y. Wang, P. Lin, F. Yan, L. Chen, H. Lezec, Y. Lu, A. Agrawal, and T. Xu, Independent amplitude control of arbitrary orthogonal states of polarization via dielectric metasurfaces, *Phys. Rev. Lett.* **125**, 267402 (2020).
- [25] A. M. Steane, M. Chowdhury, and C. J. Foot, Radiation force in the magneto-optical trap, *J. Opt. Soc. Am. B* **9**, 2142 (1992).
- [26] K. Lindquist, M. Stephens, and C. Wieman, Experimental and theoretical study of the vapor-cell Zeeman optical trap, *Phys. Rev. A* **46**, 4082 (1992).
- [27] K. F. Lamee, D. R. Carlson, Z. L. Newman, S.-P. Yu, and S. B. Papp, Nanophotonic tantalum waveguides for supercontinuum generation pumped at 1560 nm, *Opt. Lett.* **45**, 4192 (2020).
- [28] D. R. Carlson, D. D. Hickstein, A. Lind, J. B. Olson, R. W. Fox, R. C. Brown, A. D. Ludlow, Q. Li, D. Westly, H. Leopardi, T. M. Fortier, K. Srinivasan, S. A. Diddams, and S. B. Papp, Photonic-chip supercontinuum with tailored spectra for counting optical frequencies, *Phys. Rev. Appl.* **8**, 014027 (2017).
- [29] D. R. Carlson, P. Hutchison, D. D. Hickstein, and S. B. Papp, Generating few-cycle pulses with integrated nonlinear photonics, *Opt. Express* **27**, 37374 (2019).
- [30] K. Beha, D. C. Cole, P. Del'Haye, A. Coillet, S. A. Diddams, and S. B. Papp, Electronic synthesis of light, *Optica* **4**, 406 (2017).
- [31] T. H. Loftus, T. Ido, M. M. Boyd, A. D. Ludlow, and J. Ye, Narrow line cooling and momentum-space crystals, *Phys. Rev. A* **70**, 063413 (2004).
- [32] S. Snigirev, A. J. Park, A. Heinz, I. Bloch, and S. Blatt, Fast and dense magneto-optical traps for strontium, *Phys. Rev. A* **99**, 063421 (2019).
- [33] H. Katori, T. Ido, Y. Isoya, and M. Kuwata-Gonokami, Magneto-optical trapping and cooling of strontium atoms down to the photon recoil temperature, *Phys. Rev. Lett.* **82**, 1116 (1999).
- [34] T. Bothwell, W. Brand, R. Fasano, T. Akin, J. Whalen, T. Grogan, Y.-J. Chen, M. Pomponio, T. Nakamura, B. Rauf, I. Baldoni, M. Giunta, R. Holzwarth, C. Nelson, A. Hati, F. Quinlan, R. Fox, S. Peil, and A. Ludlow, Deployment of a transportable Yb optical lattice clock, *Opt. Lett.* **50**, 646 (2025).